JACS
JOURNAL OF THE AMERICAN CHEMICAL SOCIETY

ARTICLE

pubs.acs.org/JACS

Design and Synthesis of a New Class of Membrane-Permeable Triazaborolopyridinium Fluorescent Probes

Sudath Hapuarachchige,[†] Gilbert Montaño,[‡] Chinnasamy Ramesh,[†] Delany Rodriguez,[‡] Lauren H. Henson,[‡] Casey C. Williams,[‡] Samuel Kadavakkollu,[†] Dennis L. Johnson,[†] Charles B. Shuster,[‡] and Jeffrey B. Arterburn*[,†]

[†]Department of Chemistry and Biochemistry and [‡]Department of Biology, New Mexico State University, MSC 3C, Las Cruces, New Mexico 88003, United States

Supporting Information

ABSTRACT: A new class of fluorescent triazaborolopyridinium compounds was synthesized from hydrazones of 2-hydrazinylpyridine (HPY) and evaluated as potential dyes for live-cell imaging applications. The HPY dyes are small, their absorption/emission properties are tunable through variation of pyridyl or hydrazone substituents, and they offer favorable photophysical characteristics featuring large Stokes shifts and general insensitivity to solvent or pH. The stability, neutral charge, cell membrane permeability, and favorable relative influences on the water solubility of HPY conjugates are complementary to existing fluorescent dyes and offer advantages for the development of receptor-targeted small-molecule probes. This potential was assessed through the development of a new class of cysteine-derived HPY-conjugate imaging agents for the kinesin spindle protein (KSP) that is expressed in the cytoplasm during mitosis and is a promising chemotherapeutic target. Conjugates possessing the neutral HPY or charged Alexa Fluor dyes that function as potent, selective allosteric inhibitors of the KSP motor were compared using biochemical and cell-based phenotypic assays and live-cell imaging. These results demonstrate the effectiveness of the HPY dye moiety as a component of probes for an intracellular protein target and highlight the importance of dye structure in determining the pathway of cell entry and the overall performance of small-molecule conjugates as imaging agents.

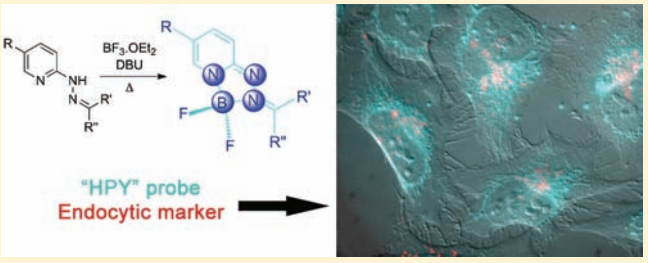

INTRODUCTION

Fluorescent compounds serve as versatile tools for molecular and cellular imaging, flow cytometry, and a wide variety of applications in biology and biotechnology.[1] The development of modular approaches, whereby different reporter groups can be conjugated to the targeting agent, is well-suited for specific applications and benefits from the availability of structurally diverse fluorescent dyes with different spectroscopic properties. Biomolecules such as DNA, proteins, and antibodies are routinely labeled with fluorescent dyes that match the required spectroscopic properties of the application, frequently involving derivatives such as fluorescein, rhodamine, and boron dipyrromethene (BODIPY) (Figure 1).[2] Advances in chemical biology and molecular library screening approaches provide exceptional opportunities for the rapid identification of novel small-molecule ligands with high affinity and selectivity for biological targets of interest and the discovery of new fluorescent scaffolds.[3] The structure and physicochemical properties of the dye-conjugate are key considerations for preservation of the targeting characteristics of the small-molecule ligand conjugates. The development of agents for intracellular targets is faced with additional challenges, since access to the corresponding intracellular compartments must be achieved by simple permeation, active transport, or endocytotic mechanisms. The large size, polycyclic aromatic structures, and presence of charged functional groups in many fluorescent dyes present major challenges when applied to the development of imaging agents based on small molecules, where the physicochemical properties of the dye may dramatically alter the solubility, biodistribution, and binding properties of the conjugate.[4] The ideal reporter dye should have characteristics that include ease and versatility of methods for attachment to small-molecule targeting agents, efficient cellular uptake, and lack of inherent biological activity or toxicity. The propensity of existing dyes to localize in specific sites or organelles is an additional factor that must be recognized and considered when designing dye-conjugates. Therefore, a significant need exists for the development of new small, neutral biocompatible fluorescent cores that exhibit good aqueous solubility, membrane permeability, favorable photophysical properties, and versatile coupling chemistries that yield minimal perturbation of targeting properties. The spectroscopic characteristics must be compatible with the instrumentation used for detection, and the fluorescent output of the probe must be

Received: January 18, 2011
Published: April 07, 2011

dx.doi.org/10.1021/ja2005175 | J. Am. Chem. Soc. 2011, 133, 6780–6790

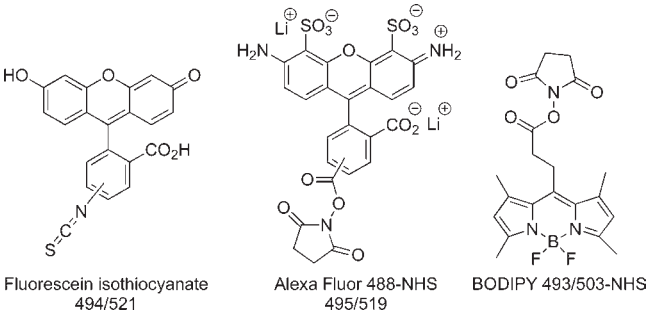

Figure 1. Structures of representative fluorescent dyes.

Scheme 1. Synthesis of Triazaborolopyridinium HPY Dyes

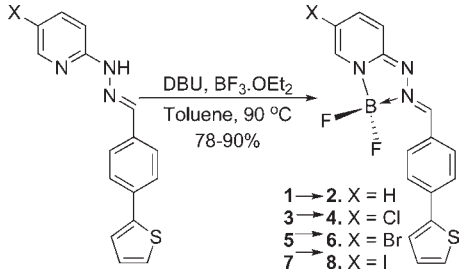

sufficient to permit the detection of the target at natural abundance levels.

We have previously used metal-mediated coupling strategies to incorporate chelates derived from the 2-hydrazinylpyridine core into estrogen derivatives for the development of ^{99m}Tc-imaging agents and became interested in the possibility of developing fluorescent dyes based on this heterocyclic scaffold.[5] Hydrazines are versatile reagents in organic and aqueous media, with rapid kinetics and favorable thermodynamics of hydrazone formation that are advantageous for bioorthogonal coupling strategies.[6] SoluLink offers proprietary technologies for bioconjugation using hydrazone formation with hydrazinylnicotinamide groups to connect proteins, DNA, antibodies, and solid surfaces.[7] The UV-traceable bis-aryl hydrazone chromophore provides a basis for quantitative determination of protein labeling using absorbance spectroscopy. Considering the versatile coupling chemistries associated with 2-hydrazinylpyridine and the promising photophysical properties associated with the extended π systems that result from hydrazone formation, we explored strategies to construct fluorescent derivatives based on this scaffold. Herein, we report the synthesis of a new class of hydrazinylpyridine-derived hydrazones (HPY) that incorporate a rigid triazaborolopyridinium core structure. The photophysical properties and initial assessment of cellular permeability suggest the suitability of HPY dyes for use as imaging probes. This potential was used to develop a new class of cysteine-derived HPY-conjugate imaging agents that function as potent, selective inhibitors of the promising chemotherapeutic target kinesin spindle protein (KSP). Comparison of fluorescent HPY and charged Alexa Fluor conjugate probes in biochemical and cell-based phenotypic assays and live-cell imaging demonstrates the importance of dye structure in determining the pathway of cell entry and the overall performance of targeted imaging agents.

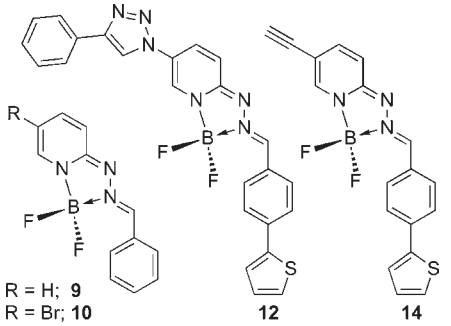

Figure 2. Structures of 5-substituted HPY dyes **9**, **10**, **12**, and **14**.

RESULTS AND DISCUSSION

Synthesis of the Fluorescent Triazaborolopyridinium Core. Hydrazin-2-ylpyridine reacts rapidly and efficiently with aldehydes and ketones to form the corresponding hydrazones. Our initial studies included the representative hydrazones **1**, **3**, **5**, and **7** derived from 4-(thiophen-2-yl)benzaldehyde (Scheme 1). These compounds exhibited strong absorption maxima in the range of 354−360 nm with molar absorptivity constants $\varepsilon \approx 38\,000$ M^{-1} cm^{-1} (Supporting Information). However, these hydrazones exhibited weak fluorescence emission spectra λ_{emi} when excited at the λ_{max} values with very low quantum yields ($\Phi_f = 6 \times 10^{-3}$). The emission was associated with relatively large Stokes shifts (~60 nm), but the low intensity precludes their use for most biological imaging applications. The simple benzaldehyde-derived hydrazone **9** (Figure 2) exhibits shifts in the absorption and emission spectra to shorter wavelength ($\lambda_{abs}/\lambda_{emi}$ 328/397 nm) and reduced quantum yield ($\Phi_f = 2 \times 10^{-3}$), consistent with expectations for a small blue shift due to loss of the extended conjugation of the 2-thiophenyl substituent.

We next considered the possible formation of cyclic systems incorporating the distal nitrogen atoms into a rigid scaffold with enforced planarity of the extended π system, anticipating that this would enhance the resulting fluorescence emission properties. Considering the basicity of the pyridin-2-yl-hydrazone moiety, we investigated the formation of Lewis acid complexes with boron trifluoride diethyl etherate. The reaction conditions for cyclization to produce the triazaborolopyridinium dyes from the hydrazone precursors used $BF_3 \cdot OEt_2$ and 1,8-diazabicyclo[5.4.0]undec-7-ene (DBU) as shown in Scheme 1 and provided yields ranging from 78 to 90%. The six-membered-ring system of the well-known 4,4-difluoro-4-bora-3a,4a-diaza-*s*-indacene (BODIPY) dyes are typically prepared from dipyrromethene intermediates under similar conditions,[2] and structural elaboration of this scaffold has yielded new analogues with modified photophysical properties.[8]

The photophysical properties of a series of HPY dyes are summarized in Table 1. The HPY compounds derived from 4-(thiophen-2-yl)benzaldehyde exhibit absorption spectra with λ_{max} 472−490 nm and molar absorptivities $\varepsilon = 26\,600-32\,900$ M^{-1} cm^{-1} in CH_3OH and emission spectra λ_{emi} 551−563 nm with characteristically large Stokes shifts (72−80 nm). These compounds exhibited high quantum yields with $\Phi_f = 0.69-0.95$. Large Stokes shifts facilitate signal detection, improve resolution by separating absorption and emission spectra, and are advantageous for imaging applications in which self-quenching must be avoided.[8d] Substituents on the 5-position of the pyridine ring were varied to identify related effects on the spectroscopic properties, since we anticipated that we would eventually use

dx.doi.org/10.1021/ja2005175 |J. Am. Chem. Soc. 2011, 133, 6780–6790

Table 1. Photophysical Properties of HPY Dyes[a]

dye[a]	λ_{max}, nm	ε, M^{-1} cm^{-1}	λ_{emi},[b] nm	Φ_f	solvent
2	472	28 800	551	0.75	MeOH
4	491	26 800	563	0.69	MeOH
6	482	32 900	562	0.95	MeOH
8	490	26 600	562	0.71	MeOH
10	471	22 600	539	0.31	MeOH
12	491	33 800	572	0.37	MeOH
14	481	36 700	572	0.38	MeOH
16	403	8 500	493	0.21	MeOH
16	404	8 600	491	0.17	1% DMSO/PBS[c]
16	408	9 300	497	0.22	CH_2Cl_2
16	403	8 600	504	0.17	acetone
16	406	9 800	500	0.07	toluene
18	400	8 300	496	0.20	MeOH
21	403	12 000	492	0.21	MeOH
21	404	12 300	492	0.16	1% DMSO/PBS[c]
21	406	11 200	497	0.20	CH_2Cl_2
21	407	10 800	504	0.23	acetone
21	410	10 600	501	0.51	toluene
22	400	9 400	476	0.21	MeOH

[a] 20 μM samples were prepared. [b] Sample was excited at λ_{max}. [c] pH 7.4.

this position for attaching targeting agents. The 5-brominated compound **6** exhibited the highest absorptivity and quantum yield in comparison with the parent scaffold **2** and the chlorinated and iodinated halogen congeners **4** and **8**, respectively (Scheme 1). The 1,2,3-triazole and ethyne derivatives **12** and **14** were selected to represent possible functional group substitutions on the pyridine backbone that could be elaborated to provide connecting linkages in small-molecule probes and used for bioorthogonal labeling strategies (Figure 2).[9] While these carbon- and nitrogen-linked derivatives produced minimal perturbation of the absorption and emission maxima, the resulting quantum yields were reduced nearly 2-fold relative to the parent compound **2**. Comparison of **6** with the simple benzaldehyde hydrazone derivative **10** reveals that the conjugated 2-thiophene group confers both longer wavelength absorption and increased quantum yield. Computational analysis of the structural effects exhibited by this series may help to identify the basis for the observed electronic trends and would provide valuable insight for further optimization of photophysical properties.

A comparison of the structure and photophysical properties of the HPY dyes with the commercially available amine-reactive fluorescent dyes fluorescein-isothiocyanate (FITC), BODIPY 493/503, and Alexa Fluor 488 provides a basis for considering the structural effects associated with small-molecule conjugates and their utility in live-cell imaging applications (Figure 1). These commercial dyes exhibit strong absorption and emission properties and are available with reactive isothiocyanate or *N*-hydroxysuccinimidyl ester (NHS) groups to facilitate their conjugation to amines. The BODIPY and HPY dyes each incorporate a heterocyclic boron-containing ring system; however, they differ in their respective six- or five-membered-ring sizes and the inclusion of additional polar nitrogen atoms in the HPY dyes. Aza-dipyrromethene analogues incorporating a nitrogen in the backbone have been described recently.[8e,f] The BODIPY and HPY dyes are electronically neutral, and BODIPY dyes have demonstrated their ability to effectively cross cell membranes

Scheme 2. Synthesis of HPY Dyes 16 and 18

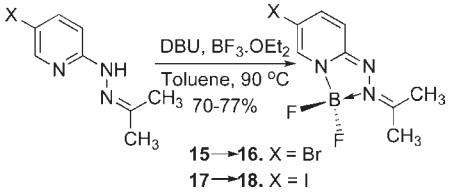

Scheme 3. Synthesis of HPY Dyes 21 and 22

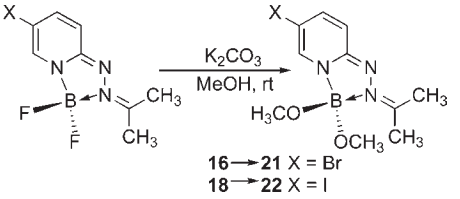

and preferentially interact with lipophilic components. While the relatively narrow emission bandwidth of the BODIPY dyes provides an intense signal, the small associated Stokes shift may require that they be excited or detected at suboptimal wavelengths, which limits the capacity to fully utilize their intense absorption/emission properties. In contrast, the HPY dyes exhibit much larger Stokes shifts and increased resolution of absorption/emission spectra (see Figure 2.3.12 in the Supporting Information). The FITC and Alexa Fluor dyes present larger relative steric profiles and consist of a mixture of two regioisomers, although single-isomer products are now commercially available. The Alexa Fluor dyes are charged at physiological pH, due to the multiple anionic sulfate and carboxylate groups. The ionic charge increases water solubility but reduces membrane permeability.

We were interested in optimizing the core structure of the HPY dyes for potential biological applications, intending to further reduce the steric profile and molecular weight while also increasing water solubility without having to introduce charged groups that would compromise membrane permeability. We elected to eliminate the hydrophobic aryl hydrazone group while retaining the 5-halogen substituent as a potential site for connecting linkages to biological targeting entities. The 2-hydrazinylpyridines react rapidly with acetone to form the corresponding hydrazone derivatives **15** and **17**, which underwent cyclization to form the 5-bromo- and 5-iodo-substituted triazaborolopyridinium compounds **16** and **18** under similar conditions (Scheme 2). To provide an additional parameter for structural modification, we investigated the possibility of replacing the fluoride substituents attached to boron with alkoxide ligands and found that this transformation occurred efficiently using mildly basic conditions in methanol to produce the stable bis-methoxide compounds **21** and **22**, respectively (Scheme 3). A related example of this type of substitution has been reported for the six-membered BODIPY dyes, although more forcing conditions involving a stepwise procedure for fluoride activation with $AlCl_3$ followed by alcohol substitution were required.[10] The acetone-derived HPY compounds **16**, **18**, **21**, and **22** were soluble in a variety of solvents, and comparison of the photophysical properties of derivatives **16** and **21** demonstrated only

dx.doi.org/10.1021/ja2005175 |*J. Am. Chem. Soc.* 2011, 133, 6780–6790

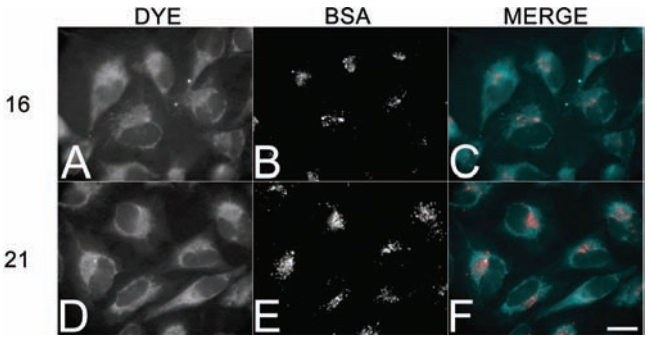

Figure 3. Membrane permeability of **16** and **21** in living HeLa cells. HeLa cells were incubated in 20 μM **16** (A−C) or **21** (D−F) for 1 h, washed free of the dye, and imaged live. Additionally, 100 μg/mL Alexa Fluor 546-labeled bovine serum albumin (BSA) was included as a marker for fluid phase endocytosis (B and E). The bar denotes 20 μm.

minor solvent-dependent variations in their absorption and emission properties in methanol, dichloromethane, acetone, toluene, and aqueous 1% DMSO in PBS buffer solution at the physiological pH 7.4 (Table 1). The acetone-derived HPY dyes required higher energy excitation (λ_{max} ~405 nm) in comparison with the aryl hydrazone derivatives, attributed to the truncated π system in these simple aliphatic derivatives. The smaller, acetone-derived hydrazone group was expected to be advantageous for increasing the relative water solubility of HPY-conjugates designed for biological applications. The absorbance/emission properties and chemical stability of **16** were unaffected over a wide range of pH (4−9) in aqueous buffer solution, such that no decomposition in solution was evident after several days at ambient temperature.

Considering the favorable characteristics of **16** and **21**, we selected these dyes to evaluate their respective cell membrane permeability and imaging properties in HeLa cells (Figure 3). To visualize the staining by conventional epifluorescence microscopy, a custom filter set was assembled that closely matched the optimal excitation/emission spectra (395/500 nm) for the two dyes in physiological buffers. Examination of cells incubated for 60 min in the presence of 20 μM **16** and **21** revealed that both dyes could be visualized throughout the cytoplasmic compartment and were particularly enriched in intracellular membranes (Figure 3A,D). To distinguish between membrane permeability and uptake by endocytosis, 100 μg/mL Alexa Fluor546 conjugated bovine serum albumin (BSA) was included to mark membrane compartments involved in endocytic trafficking (Figure 3B,E). As shown in the merged images (Figure 3C,F), the HPY dyes were distributed throughout membranous compartments that were distinct from those endosomal vesicles that contained the fluid-phase marker. The dyes **16** and **21** did not exhibit any obvious localization in specific organelles or other sites and could be removed by washing free with buffered saline. Cells treated for up to 6 h with dye concentrations of 100 μM exhibited no toxicity or other obvious effects on cell viability or phenotypic changes. Coumarin-based dyes also undergo uptake into cells without differential localization; however, sequestration in internal membranes is a common feature of many dyes such as coumarin 6 and can be washed away.[4] In contrast, rhodamine dyes 123 and B are taken up into the mitochondria, cyanine dyes often localize in the nucleus, and BODIPY dyes typically localize in the endoplasmic reticulum. These imaging results from live cells demonstrate that the triazaborolopyridinium dyes were capable of entering mammalian cells in a pathway independent of endocytosis, suggesting that these dyes were membrane-permeable and were suitable candidates for elaboration as probes for intracellular targets.

Scheme 4. Synthesis of Oxazolidine-2,5-dione 20

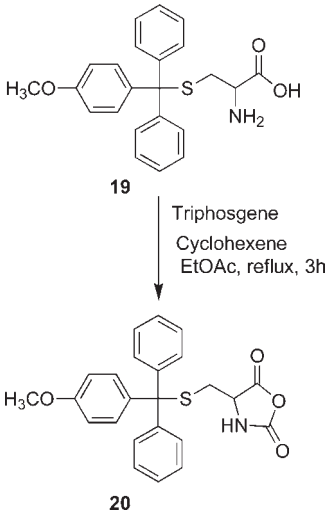

Development of Inhibitory KSP Imaging Probes. *S*-Trityl-L-cysteine is an allosteric small-molecule inhibitor of the class 5 kinesin motor kinesin spindle protein (KSP).[11] The tetrameric microtubule motor KSP plays a vital role in separating the spindle poles during mitosis, and when KSP is antagonized with small-molecule inhibitors, cells form a characteristic monopolar spindle, resulting in mitotic arrest and eventual cell death by apoptosis.[12] The development of small-molecule inhibitors as probes has played an invaluable role in the study of the cytoskeleton.[13] Fluorescent ATP-substrate analogues have been used to investigate kinesin motor function,[14] but no examples of fluorescent inhibitors have been reported. Because KSP functions only in the cytoplasm during mitosis, an inhibitory dye conjugate would not only serve as a potential imaging probe but would also provide an independent measure of the membrane permeability and performance of the synthetic triazaborolopyridinium probes.

Structure−activity analyses have identified the triphenylmethyl-mercapatoethanamine moiety as the primary pharmacaphore in this class of KSP inhibitor, and the 4′-methoxy derivative **19** was found to exhibit increased potency in biochemical and cellular assays.[11] Consideration of possible sites for the attachment of a dye to **19** requires that the resulting fluorescent conjugates retain the high-affinity allosteric binding interaction. Docking studies have suggested that the carboxylic acid group projects outside of the hydrophobic binding pocket and is not required for binding, and amide derivatives were shown to retain inhibitory activity; therefore, we selected this position for derivatization.[11b] The α-amino acid functionality of cysteine derivative **19** can be easily converted to the amine-reactive oxazolidine-2,5-dione group **20**, which provides a viable synthetic route for developing carboxamide-linked selective fluorescent inhibitors of KSP (Scheme 4).

The iodide substituted difluoro- and bis-methoxy-HPY dyes **18** and **22** were converted to the amine-functionalized alkyne products **23** and **24** in excellent yields (≥95%) by Sonogashira

dx.doi.org/10.1021/ja2005175 |*J. Am. Chem. Soc.* 2011, 133, 6780–6790

coupling of *tert*-butylbut-3-ynylcarbamate. Deprotection of the ^{t}Boc group using TFA/CH_2Cl_2 followed by neutralization of the acidic reaction mixture with triethylamine provided the corresponding primary amines, which were immediately coupled with oxazolidine-2,5-dione **20** to give the desired conjugates **25** and **26** (Scheme 5). No significant changes in the spectroscopic properties of conjugates **25** and **26** were evident in comparison to the representative HPY dyes **16** and **21** measured in 1% DMSO/PBS at pH 7.4 (Figure 4). These results demonstrate that the attachment of the triphenylmethyl substituent does not affect the photophysical properties or induce self-quenching and suggest that the distance of separation and absence of extended conjugation in the aliphatic carboxamide linkage allow the HPY dyes to function effectively as a fluorescent reporter group in conjugates **25** and **26**.

In order to compare the performance characteristics of the KSP-targeted HPY-conjugates with a representative analogue containing a commercially available fluorescent dye, we synthesized the Alexa Fluor 488 analogue **28** (Scheme 6). The amine-reactive oxazolidine-2,5-dione **20** was treated with excess 2,2′-oxybis(ethylamine) to give the monocarboxamide **27** in moderate yield. The activated *N*-hydroxysuccinimide ester of the Alexa Fluor 488 dye was coupled with the free amine of **27** to yield the desired conjugate **28**. This product was purified by reverse-phase chromatography followed by ion-exchange chromatography to provide the Na^+ salt form. The observed regioselective

Scheme 5. Synthesis of HPY-KSP Inhibitor Conjugates 25 and 26

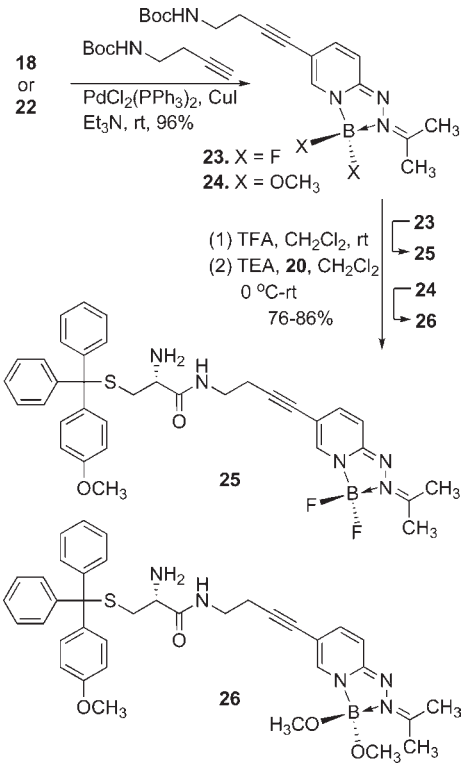

Scheme 6. Synthesis of Alexa Fluor 488-KSP Inhibitor Conjugate 28

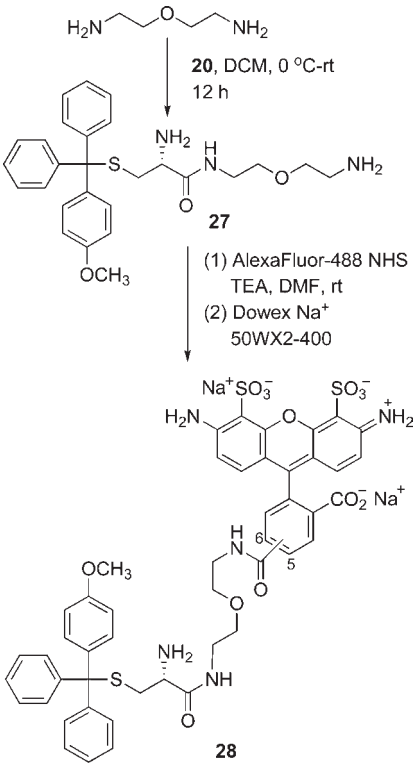

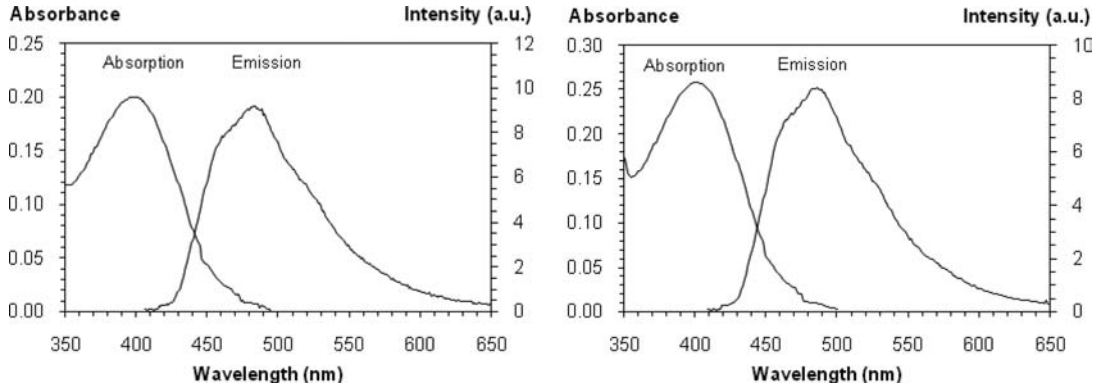

Figure 4. Absorption and emission spectra of (a) **25** (λ_{max} 400 nm, ε = 9 900 M^{-1} cm^{-1}, λ_{emi} 489 nm, Φ_f = 0.31) and (b) **26** (λ_{max} 400 nm, ε = 12 900 M^{-1} cm^{-1}, λ_{emi} = 486 nm, Φ_f = 0.29). Samples (20 μM) were prepared in 1% DMSO/PBS at pH 7.4 and 25 °C and excited at 405 nm.

dx.doi.org/10.1021/ja2005175 |*J. Am. Chem. Soc.* 2011, 133, 6780–6790

Table 2. IC_{50} Values for Inhibition of Microtubule-Stimulated KSP ATPase Activity and EC_{50} Values for Mitotic Arrest in Cell-Based Assays for Compounds 19 and 25−29[a]

compd	IC_{50}	EC_{50}
19	0.27	0.23
25	0.85	1.13
26	0.60	1.03
27	0.75	0.58
28	0.73	5.40
29	7.8	49.00

[a] Inhibitory concentrations are expressed in μM.

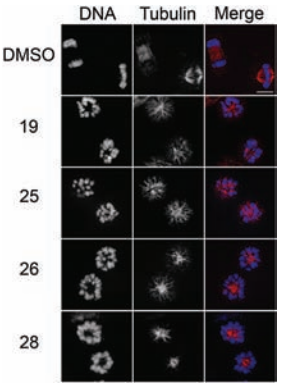

Figure 5. Fluorescent cysteine conjugates retain KSP inhibitory activity. HeLa cells were incubated in the absence or presence of 10 μM **19** or conjugates **25**, **26**, and **28** for 4 h and then fixed and probed for tubulin (red) and DNA (blue) localization. The bar denotes 10 μm.

carboxamide formation involving the sterically accessible terminal amine group was consistent with expectations for increased reactivity relative to the α-amine in **27**. Acetylation of the α-amine group of **19**, which is part of the pharmacophore, inactivates KSP inhibition.[11] Our attempts to synthesize the analogous BODIPY-493/503 conjugates following a parallel synthetic route were unsuccessful, due to major difficulties encountered in purification of the final products. These derivatives were very hydrophobic, amphiphilic compounds and tended to form intractable aggregates that were incompatible with normal or reverse-phase chromatography purification methods, and this effort was abandoned.

Characterization of KSP Inhibition. The synthetic dye conjugates **25**, **26**, and **28** were evaluated for their ability to inhibit KSP using both an in vitro biochemical assay for microtubule-stimulated ATPase activity and a cell-based assay for bipolar spindle assembly in HeLa cells (Table 2). Results of the biochemical assay using purified human KSP motor domain revealed that the original KSP inhibitor **19** exhibited a half-maximal inhibitory concentration (IC_{50}) of 0.27 μM, while the fluorescent HPY dye conjugates **25** and **26** and Alexa Fluor derivative **28** had similar IC_{50} values of 0.85, 0.60, and 0.73 μM, respectively. The IC_{50} value of the monocarboxamide derivative **27** was nearly identical with that of **28**, demonstrating that the 2,2′-oxybis(ethylamine) linkage itself had no distinct effect on KSP inhibition. These results show that each of the conjugates elicit similar inhibitory properties against the purified KSP motor, irrespective of the length of the carboxamide linkages used or the differences in size and ionic charge of the dye structures.

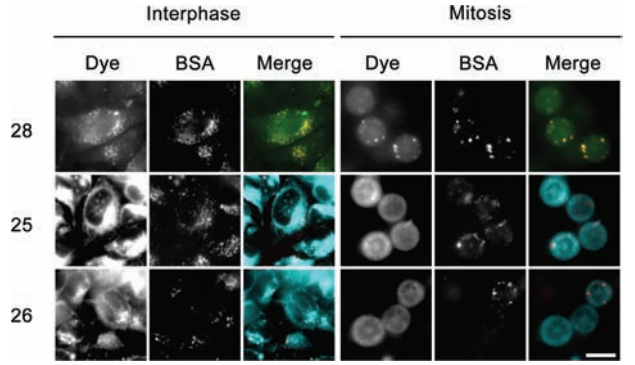

Figure 6. Imaging of fluorescent cysteine conjugates in living cells. HeLa cells were treated with fluorescent conjugates of 10 μM **25**, **26**, and **28**, coincubated with fluid-phase endocytosis marker Alexa Fluor 546-conjugated BSA for 4 h, and then imaged using wide-field epifluorescence. Fluorescence was confined to punctate structures colocalizing with the endocytosis marker (BSA) in cells treated with **28**, whereas cells treated with conjugates **25** and **26** displayed diffuse fluorescence throughout the cytoplasm. The bar denotes 20 μm.

To determine the performance of the dye-conjugated KSP inhibitors in living cells, HeLa cells were incubated in the absence or presence of 10 μM compound (**19**, **25**−**28**) for 4 h and then fixed and probed for spindle organization using antitubulin antibodies. Whereas carrier control (DMSO)-treated cells exhibited normal bipolar spindle morphology (Figure 5), cells treated with **19**, **25**, **26**, and **28** all exhibited dose-dependent formation of monopolar spindles consistent with compromised KSP activity. Comparison of the half-maximal effective concentrations (EC_{50}) for each conjugate revealed that while the HPY conjugates exhibited a 5-fold reduction in activity relative to the inhibitor **19** (Table 2), the Alexa Fluor conjugate **28** displayed a 23-fold decrease in inhibitory activity in the cell-based assay.

The observed differences in inhibitory properties of the probes in the cell-based assays can be attributed to structural differences in the attached dyes. The Alexa Fluor 488 dye is significantly larger than the HPY structure; however, the in vitro results demonstrated that there were no significant differences associated with this increased steric requirement (Table 2). The ionic charge associated with the sulfate and carboxylate groups of the Alexa Fluor 488 dye would, however, be expected to decrease the permeability across the membrane bilayer and would result in increased apparent EC_{50} values.

In order to further investigate the differences in KSP inhibition observed between the two classes of dye conjugates in the cell-based assay, the fluorescence imaging capabilities of the dye conjugates were employed to determine their subcellular distribution. HeLa cells were incubated with the dye conjugates **25**, **26**, and **28** for 4 h and then washed free of unbound dye and imaged live (Figure 6). Examination of both interphase (left panels) and mitotic cells (right panels) revealed differences in the localization patterns for the HPY and Alexa Fluor conjugates. The HPY-conjugates displayed a cytoplasmic localization that mirrored that of the free dye (Figure 3). The presence of fluoride or alkoxide substituents on boron in **25** and **26** did not affect the imaging patterns and suggests that both probes exhibit similar cellular properties. However, the Alexa Fluor derivative **28** colocalized with the fluid-phase endocytosis marker (BSA) in both interphase and mitotic cells, as shown in Figure 6. The observation that **28** retained KSP inhibitory activity in the cytoplasm was inconsistent

dx.doi.org/10.1021/ja2005175 |J. Am. Chem. Soc. 2011, 133, 6780–6790

Scheme 7. Acid Stability Study of Alexa Fluor 488-KSP Inhibitor Conjugate 28

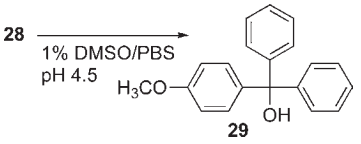

with the imaging data that suggested the Alexa Fluor dye remained sequestered within endocytic compartments and raised the possible scenario that the Alexa Fluor conjugate **28** was not stable under the acidic conditions found in the endosomal compartment.

Molecules taken up by endocytosis encounter an increasingly acidic environment as they progress through the endosomal and lysosomal compartments. The stability of Alexa Fluor conjugate **28** under conditions that resemble the acidic luminal pH of the midlate endosome (pH 4.5) was evaluated by HPLC-MS (Supporting Information, Figure 5.1). The *S*-trityl and carboxamide linkages in **28** are potential hydrolytic cleavage sites. Compound **28** underwent a time-dependent acid-catalyzed hydrolysis of the 4′-methoxytrityl group to produce the alcohol **29**, which was characterized by HPLC retention time and identified by mass spectrometry in comparison with authentic material (Scheme 7). Compound **29** was evaluated individually in the biochemical and cell-based assays, revealing that this simple trityl alcohol moiety itself exhibited KSP inhibitory properties, although it was markedly less potent than any of the corresponding thioethanamine analogues. The poor water solubility of **29** contributes to the observation of higher EC_{50} values in the cell-based assay; however, the efficiency of endocytic uptake and delivery of the charged, acid-sensitive hydrolyzable probe **28** is evident from the higher relative potency. These results, in combination with the observed subcellular localization of the Alexa Fluor fluorescence that was retained in the endocytic compartments, suggest the observed apparent KSP-inhibitory activity of conjugate **28** includes a contribution from the hydrolytic release of **29** in the acidic endosomes, which then diffuses into the cytoplasm where it inhibits KSP. In comparison, the HPY conjugates **25** and **26** are able to enter the cells via simple permeation and exhibit potent inhibitory properties in both in vitro and cell-based assays.

Consideration of dye structure is important for the design and performance of probes.[4,15] The fluorescein group is often presumed to be innocuous and permeable; however, associated effects on both transport pathway and subcellular localization have been observed in conjugates of cell-penetrating peptides.[16] A BODIPY-androgen conjugate derived from dehydroepiandrosterone mimicked the steroid in functional assays and was effective for live-cell imaging but exhibited weak uniform staining of the cytoplasm that was not displaced by competition with excess steroids and was metabolized differently.[17] A recent investigation of a series of hydrophobic tamoxifen conjugates containing Alexa Fluor, carboxyfluorescein, and BODIPY dyes revealed differences in binding affinities to estrogen receptors α and β, such that the large Alexa Fluor conjugate exhibited the weakest binding, but all three antagonized ER-mediated transcription in the nucleus with similar inhibitory IC_{50} values.[18] The Alexa Fluor conjugate exhibited slower uptake than the neutral derivatives, which is consistent with reduced permeability at short time intervals due to the charged dye. However, expectations for nuclear localization of the dyes were not realized, such that fluorescence was observed from the cytoplasm in all cases and excluded from the nucleus in ER-positive MCF7 cell lines. Attempts to identify possible cleavage products were unsuccessful but were not ruled out, due to the high probe concentrations and long incubation times involved, combined with the difficulties faced in quantifying subnanomolar concentrations of active probes. The results obtained in our investigation with Alexa Fluor conjugate **28** illustrate an important caveat for the interpretation of fluorescence localization and activity data and suggest that endocytotic uptake can serve as a route for delivering intracellular probes possessing an acid-cleavable trityl linkage.

CONCLUSIONS

The triazaborolopyridinium HPY core represents a new class of fluorescent dye that is readily synthesized from hydrazone precursors and provides complementary structural and physicochemical properties that are well suited for use in the construction of small-molecule probes. These neutral compounds are structurally related to the widely used BODIPY dyes and share favorable characteristics such as membrane permeability, and although they are not as bright, the HPY dyes exhibit larger Stokes shifts for better resolved absorption and emission spectra. The small overall size and presence of three nitrogen atoms in the conjugated heterocyclic backbone of the HPY dyes are structural factors that contribute toward favorable water solubility. The HPY dyes demonstrated tunable absorption/emission properties with variation of the hydrazone substituent, but the individual photophysical properties were relatively insensitive to varying solvents from nonpolar organic to aqueous media. The size and polarity of the hydrazone group can be easily varied, and the ability to exchange fluoride and alkoxide substituents on boron provides additional routes for structural optimization of HPY dyes for specific applications. The versatile chemistry associated with the HPY dye core structure should facilitate the construction of new fluorescent probe conjugates using a variety of synthetic strategies such as modification of the hydrazone, direct substitutions on the pyridine scaffold, or incorporation of linkages with appropriately matched reactive functional groups. In this study, we observed improved performance of the HPY-conjugated inhibitors in comparison with Alexa Fluor conjugates. Because KSP inhibitors can be used to synchronize cell cultures at G2/M, conjugates such as **25** and **26** may have broad utility as reversible probes in cell cycle research. Synthetic and computational efforts designed to further optimize the photophysical properties of the HPY scaffold, expanded comparison of additional synthetic dye conjugates, and exploration of other targeted biological imaging applications are currently in progress.

EXPERIMENTAL PROCEDURES

All compounds were synthesized in an efficient fume hood. Commercially available solvents and reagents were purchased and used without further purification. Alexa Fluor488-NHS was purchased from Invitrogen. Preparative chromatography was performed by medium-pressure column chromatography using AnaLogix SuperFlash or Sorbent Technologies RediSep C18 prepacked columns. ^{1}H NMR spectra were acquired at 300 or 400 MHz, and ^{13}C NMR spectra were acquired at 75 or 100 MHz at ambient temperature (20 ± 2 °C). ^{1}H NMR spectra in $CDCl_3$ were referred to TMS, and C_6F_6 was used as an internal reference in ^{19}F NMR spectra. The purities and molecular weights of compounds were determined by a Waters 2695 Alliance HPLC/ESI-MS instrument with a C18 reverse-phase column system and 20−70% acetonitrile in

water as eluent. High-resolution mass spectra were obtained at the University of California at Riverside.

General Procedure A for Triazaborolopyridinium Cyclization. Boron trifluoride diethyl etherate ($BF_3 \cdot OEt_2$, 5.0 equiv) was added dropwise to a mixture of the hydrazone (1.0 equiv) and DBU (3.0 equiv) in anhydrous toluene (0.02 M) at room temperature and heated at 90 °C for 1−6 h under an argon atmosphere. The reaction mixture was quenched with water (5.0 mL), and the product was extracted with CH_2Cl_2 (2 × 50 mL). The combined organic layers were washed with water (3 × 50 mL), dried over anhydrous Na_2SO_4, and evaporated under reduced pressure. The solid residue was purified by silica gel column chromatography using CH_3OH/CH_2Cl_2 (0−1%) as the eluent.

General Procedure B for Methoxide Substitution. The fluorinated HPY dye (1.0 equiv) was dissolved in methanol (2.0 M) and treated with K_2CO_3 (2.2 equiv). The mixture was stirred for 2 h and diluted with CH_2Cl_2 (100 mL). The organic layer was washed with water (3 × 50 mL) and dried over anhydrous Na_2SO_4. Volatiles were removed under reduced pressure, and the residue was dried in vacuo. The solid residue was purified by reverse-phase C18 column chromatography using CH_3CN/H_2O (20−50%) as the eluent.

3,3-Difluoro-2-(4-(thiophen-2-yl)benzylidene)-2,3-dihydro-[1,2,4,3]triazaborolo[4,5-*a*]pyridin-2-ium-3-uide (2). The reaction was performed following the general procedure A for 5 h starting with **1** (0.056 g, 0.2 mmol). The product **2** (0.051 g, 78%) was obtained as a red solid. ^{1}H NMR (400 MHz, DMSO-d_6): δ 8.67 (s, 1H), 8.05 (d, J = 8.48 Hz, 2H), 7.86 (d, J = 8.48 Hz, 2H), 7.74 (dd, J = 3.32, 1.06 Hz, 1H), 7.69 (dd, J = 5.02, 1.06 Hz, 2H), 7.52 (ddd, J = 8.25, 7.67, 1.68 Hz, 1H), 7.20 (dd, J = 5.02, 3.66 Hz, 1H), 6.70 (d, J = 8.88 Hz, 1H), 6.40 (dt, J = 6.49, 6.24, 0.86 Hz, 1H). ^{13}C NMR (75 MHz, $CDCl_3$): δ 141.2, 138.9, 135.7, 133.2, 128.4, 127.2, 126.6, 126.0, 125.8, 125.3, 124.7, 123.5, 113.2, 110.2. ^{19}F NMR ($CDCl_3$): δ −150.33 (q, J = 28 Hz, 2F). FT-IR (KBr): 1641 (s), 1609 (w), 1491 (s), 1105 (m), 1023 (w) cm^{-1}. HPLC/ESI-MS (m/z): calcd for $C_{16}H_{13}BF_2N_3S$ $[M + H]^+$ 328.09, found 328.19.

6-Chloro-3,3-difluoro-2-(4-(thiophen-2-yl)benzylidene)-2,3-dihydro[1,2,4,3]triazaborolo[4,5-*a*]pyridin-2-ium-3-uide (4). The reaction was performed following the general procedure A for 3 h starting with **3** (0.063 g, 0.2 mmol). The product **4** (0.057 g, 78%) was obtained as a red solid. ^{1}H NMR (300 MHz, $CDCl_3$): δ 8.33 (s, 1H), 7.98−7.94 (m, 2H), 7.75−7.71 (m, 2H), 7.46 (dd, J = 3.74, 1.14 Hz, 1H), 7.45 (s, 1H), 7.39 (dd, J = 5.06, 1.02 Hz, 1H), 7.29 (d, J = 2.31 Hz, 1H), 7.13 (dd, J = 5.10, 4.23 Hz, 1H), 6.60 (d, J = 9.64 Hz, 1H). ^{13}C NMR (100 MHz, DMSO-d_6): δ 154.5, 144.2, 142.8, 140.6, 138.8, 134.2, 133.9, 128.6, 127.1, 126.1, 125.6, 124.2, 120.4, 108.6. ^{19}F NMR ($CDCl_3$): δ −150.4 (q, J = 28 Hz, 2F). FT-IR (KBr): 1645 (w), 1597 (w), 1491 (s), 1133 (m), 1059 (m) cm^{-1}. HPLC/ESI-MS (m/z): calcd for $C_{16}H_{12}BClF_2N_3S$ $[M + H]^+$ 362.05, found 362.32.

6-Bromo-3,3-difluoro-2-(4-(thiophen-2-yl)benzylidene)-2,3-dihydro[1,2,4,3]triazaborolo[4,5-*a*]pyridin-2-ium-3-uide (6). The reaction was performed following the general procedure A for 3 h starting with **5** (0.085 g, 0.24 mmol). The product **6** (0.090 g, 90%) was obtained as a red solid. ^{1}H NMR (300 MHz, $CDCl_3$): δ 8.42−8.39 (m, 2H), 7.78−7.75 (m, 2H), 7.67 (s, 1H), 7.50−7.45 (m, 3H), 7.40 (d, J = 5.12 Hz, 1H), 7.14 (dd, J = 4.90, 3.81 Hz, 1H), 6.77 (d, J = 9.51 Hz, 1H). ^{13}C NMR (75 MHz, $CDCl_3$): δ 143.8, 143.0, 140.6, 138.1, 136.1, 133.5, 128.8, 128.5, 126.8, 126.0, 125.8, 124.9, 114.6, 102.7. ^{19}F NMR ($CDCl_3$): δ −149.4 (q, J = 28 Hz, 2F). FT-IR (KBr): 1641 (m), 1605 (w), 1526 (m), 1498 (s), 1048 (m) cm^{-1}. HPLC/ESI-MS (m/z): calcd for $C_{16}H_{12}BBrF_2N_3S$ $[M + H]^+$ 406.00, found 406.04.

6-Iodo-3,3-difluoro-2-(4-(thiophen-2-yl)benzylidene)-2,3-dihydro[1,2,4,3]triazaborolo[4,5-*a*]pyridin-2-ium-3-uide (8). The reaction was performed following the general procedure A for 3 h starting with **7** (0.061 g, 0.15 mmol). The product **8** (0.054 g, 80%) was obtained as a red solid. ^{1}H NMR (300 MHz, $CDCl_3$): δ 8.42 (m, 1H), 8.39 (m, 1H), 7.77 (m, 2H), 7.74 (m, 1H), 7.56 (ddd, J = 9.12, 1.77, 1.66 Hz, 1H), 7.50−7.47 (m, 2H), 7.39 (d, J = 4.98 Hz, 1H), 7.14 (ddd, J = 6.77, 3.74, 1.17 Hz, 1H), 6.68 (d, J = 9.39 Hz, 1H). ^{13}C NMR (75 MHz, $CDCl_3$): δ 148.2, 143.0, 141.1, 140.5, 138.1, 133.6, 133.5, 128.8, 128.5, 126.8, 126.0, 125.8, 124.9, 115.0. ^{19}F NMR ($CDCl_3$): δ −149.4 (q, J = 28 Hz, 2F). FT-IR (KBr): 1634 (s), 1606 (m), 1493 (s), 1403 (m), 1147 (m) cm^{-1}. HPLC/ESI-MS (m/z): calcd for $C_{16}H_{12}BF_2IN_3S$ $[M + H]^+$ 453.99, found 454.03.

2-Benzylidene-6-bromo-3,3-difluoro-2,3-dihydro[1,2,4,3]-triazaborolo[4,5-*a*]pyridin-2-ium-3-uide (10). The reaction was performed following the general procedure A for 4 h starting with **9** (0.138 g, 0.5 mmol). The product **10** (0.133 g, 82%) was obtained as an orange solid. ^{1}H NMR (400 MHz, DMSO-d_6): δ 8.57 (d, J = 7.28 Hz, 2H), 8.22 (s, 1H), 8.05 (s, 1H), 7.77 (dd, J = 9.14, 1.78 Hz, 1H), 7.62−7.57 (m, 3H), 6.94 (d, J = 9.48 Hz, 1H). ^{13}C NMR (100 MHz, DMSO-d_6): δ 160.1, 144.6, 141.9, 136.5, 133.0, 132.8, 130.0, 128.9, 114.4, 102.8. ^{19}F NMR (DMSO-d_6): δ −145.62 (q, J = 28 Hz, 2F). FT-IR (KBr): 1643 (m), 1608 (w), 1489 (s), 1405 (m), 1143 (m) cm^{-1}. HPLC/ESI-MS (m/z): calcd for $C_{12}H_{10}BBrF_2N_3$ $[M + H]^+$ 324.01, found 324.07.

3,3-Difluoro-6-(4-phenyl-1*H*-1,2,3-triazol-1-yl)-2-(4-(thiophen-2-yl)benzylidene)-2,3-dihydro[1,2,4,3]triazaborolo-[4,5-*a*]pyridin-2-ium-3-uide (12). The reaction was performed following the general procedure A for 3 h starting with **11** (0.018 g, 0.043 mmol). The product **12** (0.018 g, 87%) was obtained as a red solid. ^{1}H NMR (300 MHz, DMSO-d_6): δ 9.20 (s, 1H), 8.63 (s, 1H), 8.60 (s, 1H), 8.58 (d, J = 1.89 Hz, 1H), 8.21 (dd, J = 9.69, 2.34 Hz, 1H), 8.14 (s, 1H), 7.93−7.88 (m, 4H), 7.77 (dd, J = 3.66, 1.02 Hz, 1H), 7.71 (dd, J = 5.06, 1.17 Hz, 1H), 7.53−7.48 (m, 2H), 7.41−7.35 (m, 1H), 7.23−7.18 (m, 2H). ^{13}C NMR (75 MHz, DMSO-d_6): δ 147.2, 142.3, 142.1, 137.8, 136.0, 134.1, 130.2, 129.2, 129.1, 128.9, 128.7, 128.5, 128.4, 128.2, 126.2, 125.5, 125.4, 123.5, 120.1, 114.1. ^{19}F NMR ($CDCl_3$): δ −148.4 (q, J = 28 Hz, 2F). FT-IR (KBr): 1655 (w), 1614 (m), 1519 (m), 1137 (w), 1025 (m) cm^{-1}. HPLC/ESI-MS (m/z): calcd for $C_{24}H_{18}BF_2N_6S$ $[M + H]^+$ 471.14, found 471.41.

6-Ethynyl-3,3-difluoro-2-(4-(thiophen-2-yl)benzylidene)-2,3-dihydro[1,2,4,3]triazaborolo[4,5-*a*]pyridin-2-ium-3-uide (14). The reaction was performed following the general procedure A for 1 h starting with **9** (0.112 g, 0.37 mmol). The product **14** (0.107 g, 83%) was obtained as a red solid. ^{1}H NMR (400 MHz, $CDCl_3$): δ 8.35 (s. 1H), 7.98−7.96 (m, 2H), 7.75−7.73 (m, 2H), 7.64 (m, 1H), 7.47 (dd, J = 3.72, 1.08 Hz, 1H), 7.40 (dd, J = 5.02, 1.07 Hz, 1H), 7.34 (dd, J = 9.38, 1.85 Hz, 1H), 7.14 (dd, J = 5.07, 3.62 Hz, 1H), 6.58 (d, J = 9.37 Hz, 1H), 3.05 (s, 1H). ^{13}C NMR (75 MHz, $CDCl_3$): δ 153.4, 143.2, 142.9, 140.0, 138.2, 137.0, 133.6, 128.5, 126.9, 125,8, 125.0, 117.2, 117.2, 113.1, 79.3, 78.5. ^{19}F NMR ($CDCl_3$): δ −150.01 (q, J = 28 Hz, 2F). FT-IR (KBr): 2112 (m), 1644 (s), 1609 (w), 1509 (s), 1044 (m) cm^{-1}. HPLC/ESI-MS (m/z): calcd for $C_{18}H_{13}BF_2N_3S$ $[M + H]^+$ 352.09, found 352.12.

6-Bromo-3,3-difluoro-2-(propan-2-ylidene)-2,3-dihydro-[1,2,4,3]triazaborolo[4,5-*a*]pyridin-2-ium-3-uide (16). The reaction was performed following the general procedure A for 6 h using **15** (0.146 g, 0.64 mmol). The product **16** (0.107 g, 60%) was obtained as a greenish yellow solid. ^{1}H NMR (300 MHz, DMSO-d_6): δ 7.82 (d, J = 1.32 Hz, 1H), 7.46 (dd, J = 9.69, 2.20 Hz, 1H), 6.69 (dd, J = 9.53 Hz, 1H), 2.36 (s, 3H), 2.32 (s, 3H). ^{13}C NMR (75 MHz, DMSO-d_6): δ 166.3, 157.8, 142.8, 135.3, 113.6, 99.7, 21.2, 21.0. ^{19}F NMR (DMSO-d_6): δ −145.81 (q, J = 28 Hz, 2F). FT-IR (KBr): 1658 (w), 1625 (m), 1498 (s), 1154 (s), 1018 (m) cm^{-1}. HRMS/ESI-TOF (m/z): calcd for $C_8H_{10}BBrF_2N_3$ $[M + H]^+$ 276.0119, found 276.0114.

3,3-Difluoro-6-iodo-2-(propan-2-ylidene)-2,3-dihydro-[1,2,4,3]triazaborolo[4,5-*a*]pyridin-2-ium-3-uide (18). The reaction was performed following the general procedure A for 4 h starting

with **17** (0.235 g, 0.85 mmol). The product **18** (0.212 g, 77%) was obtained as a greenish yellow solid. ^{1}H NMR (300 MHz, $CDCl_3$): δ 7.54 (b s, 1H), 7.35 (dd, J = 9.40, 2.01, 1H), 6.41 (d, J = 9.54, 1H), 2.41 (s, 3H), 2.37 (s, 3H). ^{13}C NMR (75 MHz, $CDCl_3$): δ 163.4, 158.6, 147.0, 140.3, 114.0, 66.6, 21.6, 21.5. ^{19}F NMR ($CDCl_3$): δ −149.38 (q, J = 28 Hz, 2F). FT-IR (KBr): 1658 (w), 1619 (m), 1501 (s), 1152 (s), 1014 (m) cm^{-1}. HRMS/ESI-TOF (m/z): calcd for $C_8H_{10}BF_2IN_3$ $[M + H]^+$ 323.9975, found 323.9979.

4-(((4-Methoxyphenyl)diphenylmethylthio)methyl)-oxazolidine-2,5-dione (20). Triphosgene (0.932 g, 3.15 mmol) was added to a mixture of **19** (0.589 g, 1.5 mmol) and cyclohexene (1.23 g, 15 mmol) in ethyl acetate (10 mL) at 0 °C. The reaction mixture was heated at 85 °C for 3 h. The volatiles were removed in vacuo. The residue was dissolved in CH_2Cl_2 (20 mL) and washed with water (35 mL). The organic layer was dried over anhydrous Na_2SO_4 and concentrated under reduced pressure to isolate the product **20** (0.525 g, 84%) as a colorless solid. This compound was used directly in subsequent reactions or could be stored at 5 °C under anhydrous conditions for up to 2 days. ^{1}H NMR (300 MHz, $CDCl_3$): δ 7.53−7.08 (m, 12H), 6.93−6.73 (m, 2H), 5.15 (s, 1H), 3.80 (s, 3H), 3.58−3.51 (dd, J = 8.51, 3.96 Hz, 1H), 2.87−2.68 (m, 2H); ^{13}C NMR (75 MHz, $CDCl_3$): δ 167.85, 158.43, 151.17, 144.00, 135.65, 130.58, 129.22, 128.24, 127.15, 113.50, 67.28, 56.53, 55.26, 33.27. FT-IR (KBr, cm^{-1}): 3399 (s), 1860 (s), 1785 (m), 1601 (w), 1508 (w).

6-Bromo-3,3-dimethoxy-2-(propan-2-ylidene)-2,3-dihydro-[1,2,4,3]triazaborolo[4,5-*a*]pyridin-2-ium-3-uide (21). The reaction was performed following the general procedure B starting with **16** (0.028 g, 0.1 mmol) and a reaction time of 3.5 h. The solid residue was purified by reverse-phase column chromatography with CH_3CN/H_2O (50/50) as the eluent to isolate the product **21** (0.023 g, 77%) as a greenish yellow solid. ^{1}H NMR (300 MHz, $CDCl_3$): δ 7.37 (dd, J = 2.06, 0.74 Hz, 1H), 7.25 (dd, J = 9.53, 1.76 Hz, 1H), 6.48 (dd, J = 9.53, 0.73 Hz, 1H), 3.07 (s, 6H), 2.38 (s, 3H), 2.36 (s, 3H). ^{13}C NMR (75 MHz, $CDCl_3$): δ 160.4, 159.0, 142.0, 135.9, 113.2, 100.1, 49.9, 21.3, 20.5. FT-IR (KBr): 1650 (m), 1619 (m), 1528 (m), 1500 (s), 1222 (m) cm^{-1}. HRMS/ESI-TOF (m/z): calcd for $C_{10}H_{16}BBrN_3$ $[M + H]^+$ 300.0519, found 300.0513.

6-Iodo-3,3-dimethoxy-2-(propan-2-ylidene)-2,3-dihydro-[1,2,4,3]triazaborolo[4,5-*a*]pyridin-2-ium-3-uide (22). The reaction was performed following the general procedure B starting with **18** (0.097 g, 0.3 mmol) and a reaction time of 3.5 h. The solid residue was purified by reverse-phase flash chromatography with CH_3CN/H_2O (20/80) as eluent to isolate the product **22** (0.096 g, 90%) as a greenish yellow solid. ^{1}H NMR (300 MHz, $CDCl_3$): δ 7.47 (dd, J = 2.00, 0.80 Hz, 1H), 7.35 (dd, J = 9.39, 2.06 Hz, 1H), 6.41 (dd, J = 9.39, 0.88 Hz, 1H), 3.07 (s, 6H), 2.38 (s, 3H), 2.36 (s, 3H). ^{13}C NMR (75 MHz, $CDCl_3$): δ 160.3, 158.8, 146.3, 141.0, 113.7, 66.4, 50.0, 21.3, 20.5. FT-IR (KBr): 1651 (m), 1615 (m), 1523 (m), 1498 (s), 1219 (s) cm^{-1}. HRMS/ESI-TOF (m/z): calcd for $C_{10}H_{16}BBrN_3O_2$ $[M + H]^+$ 348.0375, found 348.0372.

6-(4-(*tert*-Butoxycarbonylamino)but-1-ynyl)-3,3-difluoro-2-(propan-2-ylidene)-2,3-dihydro[1,2,4,3]triazaborolo[4,5-*a*]-pyridin-2-ium-3-uide (23). A mixture of **18** (0.134 g, 0.42 mmol), Boc-but-3-yn-1-amine (0.141 g, 0.83 mmol), $PdCl_2(PPh_3)_2$ (14.6 mg, 2.07×10^{-2} mmol), and CuI (4.0 mg, 2.07×10^{-2} mmol) in Et_3N (4 mL) was stirred for 2 h at ambient temperature under an argon atmosphere. Volatiles were removed in vacuo. The solid residue was dissolved in CH_2Cl_2 (10 mL) and filtered through a plug of Celite. The filtrate was concentrated, and the residue was purified by silica gel column chromatography using CH_3OH/CH_2Cl_2 (0−0.5%) to isolate the product **23** (0.147 g, 96%) as a greenish yellow solid. ^{1}H NMR (300 MHz, $CDCl_3$): δ 7.47 (s, 1H), 7.21 (dd, J = 9.30, 1.80 Hz, 1H), 6.51 (d, J = 9.39 Hz, 1H), 4.83 (bs, 1H), 3.32 (dt, J = 6.44, 6.31 Hz, 2H), 2.55 (t, J = 6.46, 2H), 2.42 (s, 3H), 2.37 (s, 3H), 1.46 (s, 9H). ^{13}C NMR (75 MHz, $CDCl_3$): δ 163.1, 158.7, 155.7, 142.3, 138.2, 111.8, 104.3, 87.3, 79.5, 77.8, 39.5, 28.4, 21.5, 21.4, 21.0. ^{19}F NMR ($CDCl_3$): δ −149.94 (q, J = 28 Hz, 2F). FT-IR (neat): 3300 (b), 2171 (w), 1650 (m), 1510 (s), 1110 (m) cm^{-1}. HPLC/ESI-MS (m/z): calcd for $C_{17}H_{24}BF_2N_4O_2$ $[M + H]^+$ 365.20, found 365.30.

6-(4-(*tert*-Butoxycarbonylamino)but-1-ynyl)-3,3-dimethoxy-2-(propan-2-ylidene)-2,3-dihydro[1,2,4,3]triazaborolo[4,5-*a*]-pyridin-2-ium-3-uide (24). The mixture of **22** (0.069 g, 0.2 mmol), Boc-but-3-yn-1-amine (0.068 g, 0.4 mmol), $PdCl_2(PPh_3)_2$ (7.0 mg, 1.0×10^{-2} mmol), and CuI (1.9 mg, 1.0×10^{-2} mmol) in Et_3N (4 mL) was stirred for 2 h at ambient temperature under an argon atmosphere. Volatiles were evaporated under reduced pressure. The solid residue was dissolved in CH_2Cl_2 (10 mL) and this solution filtered through a plug of Celite. The filtrate was concentrated, and the residue was purified by silica gel column chromatography using CH_3OH/CH_2Cl_2 (0−1.0%) to isolate the product **24** (0.074 g, 95%) as a greenish yellow solid. ^{1}H NMR (300 MHz, $CDCl_3$): δ 7.47 (d, J = 1.00 Hz, 1H), 7.21 (dd, J = 9.39, 1.91 Hz, 1H), 6.51 (dd, J = 9.39, 0.90 Hz, 1H), 4.85 (bs, 1H), 3.33 (dt, J = 6.30, 6.17 Hz, 2H), 3.06, (s, 6H), 2.57 (t, J = 6.60 Hz, 2H), 2.39 (s, 3H), 2.36 (s, 3H), 1.46 (s, 9H). ^{13}C NMR (75 MHz, $CDCl_3$): δ 160.3, 158.9, 155.7, 141.6, 139.0, 111.5, 103.8, 87.2, 79.5, 78.2, 49.9, 39.5, 28.4, 21.3, 21.0, 20.5. FT-IR (neat): 3259 (b), 2167 (w), 1630 (m), 1510 (s), 1141 (m) cm^{-1}. HPLC/ESI-MS (m/z): calcd for $C_{19}H_{30}BN_4O_2$ $[M + H]^+$ 389.24, found 389.16.

6-(4-(2-Amino-3-((4-methoxyphenyl)diphenylmethylthio)-propanamido)but-1-ynyl)-3,3-difluoro-2-(propan-2-ylidene)-2,3-dihydro[1,2,4,3]triazaborolo[4,5-*a*]pyridin-2-ium-3-uide (25). Trifluoroacetic acid (TFA, 50 μL) was added dropwise to compound **23** (0.026 g, 0.07 mmol) in methylene chloride (1.0 mL) and stirred for 3 h at ambient temperature under an argon atmosphere. The mixture was diluted with CH_2Cl_2 (2 mL), cooled in an ice bath, and neutralized by dropwise addition of Et_3N (90 μL). The cyclic anhydride oxazolidine-2,5-dione **20** (0.036 g, 0.089 mmol) in CH_2Cl_2 (2 mL) was added to the neutralized reaction mixture dropwise over 15 min, and this mixture was stirred for 3 h at 0 °C to room temperature under an argon atmosphere. The reaction mixture was diluted with CH_2Cl_2 (100 mL). The organic layer was washed with saturated NH_4Cl (2 × 50 mL), saturated $NaHCO_3$ (2 × 50 mL), and H_2O (3 × 50 mL) and dried over anhydrous Na_2SO_4. Volatiles were evaporated under reduced pressure, and the solid residue was purified by silica gel column chromatography using CH_3OH/CH_2Cl_2 (0−1%) to isolate the product **25** (0.039 g, 86%) as a greenish yellow solid. ^{1}H NMR (300 MHz, $CDCl_3$): δ 7.45−7.28 (m, 10H), 7.23−7.14 (m, 4H), 6.81 (d, J = 9.10 Hz, 2H), 6.48 (d, J = 9.39 Hz, 1H), 3.78 (s, 3H), 3.76 (m, 1H), 3.43−3.28 (m, 2H), 3.06 (dd, J = 8.37, 3.96 Hz, 1H), 2.74 (dd, J = 12.60, 4.02 Hz, 1H), 2.62−2.50 (m, 3H), 2.42 (s, 3H), 2.37 (s, 3H), 1.60 (b s, 2H). ^{13}C NMR (75 MHz, $CDCl_3$): δ 172.9, 163.1, 158.7, 158.2, 144.9, 144.7, 142.2, 138.2, 136.6, 130.7, 129.5, 127.9, 126.7, 113.2, 111.8, 104.3, 87.2, 77.9, 66.5, 55.2, 54.0, 37.9, 37.3, 21.5, 20.4. ^{19}F NMR ($CDCl_3$): −149.88 (q, J = 28 Hz, 2F). FT-IR (neat): 3360 (b), 2120 (w), 1680 (m), 1510 (m), 1110 (m) cm^{-1}. HRMS/ESI-TOF (m/z): calcd for $C_{35}H_{36}BF_2N_5NaO_2S$ $[M + Na]^+$ 662.2543, found 662.2537.

6-(4-(2-Amino-3-((4-methoxyphenyl)diphenylmethylthio)-propanamido)but-1-ynyl)-3,3-dimethoxy-2-(propan-2-ylidene)-2,3-dihydro[1,2,4,3]triazaborolo[4,5-*a*]pyridin-2-ium-3-uide (26). Trifluoroacetic acid (TFA, 50 μL) was added dropwise to compound **24** (0.027 g, 0.07 mmol) in CH_2Cl_2 (1.0 mL), and the mixture was stirred for 3 h at room temperature under an argon atmosphere. The mixture was diluted with CH_2Cl_2 (2 mL), cooled in an ice bath, and neutralized by dropwise addition of Et_3N (90 μL). The oxazolidine-2, 5-dione **20** (0.038 g, 0.09 mmol) in CH_2Cl_2 (2 mL) was added to the neutralized reaction mixture dropwise over 15 min and stirred for 3 h at 0 °C to room temperature under an argon atmosphere. The reaction

mixture was diluted with CH_2Cl_2 (100 mL). The organic layer was washed with saturated NH_4Cl (2 × 50 mL), saturated $NaHCO_3$ (2 × 50 mL), and H_2O (3 × 50 mL) and dried over anhydrous Na_2SO_4. Volatiles were evaporated under reduced pressure, and the solid residue was purified by silica gel column chromatography using CH_3OH/CH_2Cl_2 (0−1%) to isolate the product **26** (0.035 g, 76%) as a greenish yellow solid. ^{1}H NMR (300 MHz, $CDCl_3$): δ 7.45−7.28 (m, 10H), 7.25−7.15 (m, 4H), 6.81 (d, J = 9.09 Hz, 2H), 6.49 (dd, J = 9.39, 0.90 Hz, 1H), 3.79 (s, 3H), 3.77−3.25 (m, 1H), 3.42−3.29 (m, 2H), 3.08−3.02 (m, 7H), 2.73 (dd, J = 12.75, 3.96 Hz, 1H), 2.61−2.51 (m, 3H), 2.39 (s, 3H), 2.39 (s, 3H), 1.60 (b s, 2H). ^{13}C NMR (75 MHz, $CDCl_3$): δ 173.0, 160.4, 158.9, 158.2, 144.9, 144.7, 141.6, 139.0, 136.5, 130.8, 129.5, 127.9, 126.7, 113.2, 111.5, 103.8, 86.9, 78.4, 66.5, 55.2, 54.0, 49.9, 37.9, 37.4, 21.3, 20.4. FT-IR (KBr): 3270 (b), 2110 (w), 1689 (m), 1510 (s), 1140 (m) cm^{-1}. HRMS/ESI-TOF (m/z): calcd for $C_{37}H_{43}BN_5O_4S$ $[M + H]^+$ 664.3123, found 664.3121.

2-Amino-*N*-(2-(2-aminoethoxy)ethyl)-3-((4-methoxyphenyl)diphenylmethylthio)propanamide (27). The oxazolidine-2,5-dione **20** (0.105 g, 0.25 mmol) in CH_2Cl_2 (3 mL) was added dropwise to 2,2′-oxybis(ethylamine) in CH_2Cl_2 (3 mL) at 0 °C for 30 min, and the reaction mixture was stirred for 12 h at room temperature. The reaction mixture was diluted with CH_2Cl_2 (25 mL) and washed with H_2O. The organic layer was dried over anhydrous Na_2SO_4 and concentrated under reduced pressure. The crude residue was purified by silica gel column chromatography using CH_3OH/CH_2Cl_2 (20/80) to provide the product **27** (0.067 g, 56%) as a colorless solid. ^{1}H NMR (300 MHz, $CDCl_3$): δ 7.45−7.17 (m, 12H), 6.85 −6.75 (m, 2H), 3.78 (s, 3H), 3.55−3.30 (m, 6H), 3.10−3.00 (dd, J = 8.37, 3.97 Hz, 1H), 2.85−2.78 (t, J = 5.06 Hz, 2H), 2.76−2.67 (dd, J = 12.62, 4.11 Hz, 1H), 2.60−2.50 (dd, J = 12.62, 8.36 Hz, 1H), 1.76 (s, 2H). ^{13}C NMR (75 MHz, $CDCl_3$): δ 173.0, 158.1, 144.9, 136.6, 130.7, 129.5, 127.9, 126.7, 113.2, 72.7, 69.5, 66.4, 55.2, 54.0, 41.5, 38.9, 37.5. FTIR (KBr, cm^{-1}): 3391 (s), 2954 (m), 1658 (s), 1384 (m), 1250 (m). HPLC-MS: elution with CH_3CN/H_2O (20/80) exhibited a single peak at 4.43 min. HPLC/ESI-MS (m/z): calcd for $C_{27}H_{34}N_3O_3S$ $[M + H]^+$ 480.17, found 480.22.

Synthesis of Alexa Fluor488 Conjugate (28). To a mixture of **27** (1.0 mg, 0.002 mmol) and Et_3N (5 μL) in dry DMF (0.25 mL) was added Alexa Fluor488-NHS (1.0 mg, 0.0016 mmol) in dry DMF (0.20 mL) at 0 °C over 15 min, and this mixture was stirred at room temperature for 12 h. Volatiles were removed in vacuo, and the crude residue was purified by a reverse-phase C18 column using CH_3CN/H_2O (50/50). The fractions containing product were combined and concentrated in vacuo. A pipet column containing Dowex 50WX2-400 ion-exchange resin (1.0 g) was prepared by washing with sequential potions of H_2O (2 mL), CH_3OH (2 mL), H_2O (2 mL), 2 N NaOH (1 mL), and H_2O (2 mL), respectively. The concentrate was dissolved in water (0.5 mL) and eluted through the column; fractions containing the Na^+ salt of the product were combined and concentrated in vacuo to provide the product **28** (1.5 mg, 95%). HPLC/ESI-MS (m/z): calcd for $C_{48}H_{46}N_5O_{13}S_3$ $[M + H]^+$ 996.22, found 996.13.

■ ASSOCIATED CONTENT

Supporting Information. Text and figures giving experimental details for synthetic and biological studies, compound identity and purity characterization spectra, and the complete ref 4. This material is available free of charge via the Internet at http://pubs.acs.org.

■ AUTHOR INFORMATION

Corresponding Author
jarterbu@nmsu.edu

■ ACKNOWLEDGMENT

We thank Dr. Lori Wilmeth for her assistance in the cell culture experiments and acknowledge funding from NM-INBRE P20 RR16480, R25 GM61222, and the Cowboys for Cancer Research Foundation.

■ REFERENCES

(1) (a) Zhang, J.; Campbell, R. E.; Ting, A. Y.; Tsien, R. Y. *Nat. Rev. Mol. Cell Biol.* **2002**, *3*, 906–918. (b) Lavis, L. D.; Raines, R. T. *ACS Chem. Biol.* **2008**, *3* (3), 142–155. (c) Walter, N. G.; Huang, C. Y.; Manzo, A. J.; Sobhy, M. A. *Nature Methods* **2008**, *5* (6), 475–489. (d) Tinnefeld, P.; Sauer, M. *Angew. Chem., Int. Ed.* **2005**, *44*, 2642–2671. (e) Goncalves, M. S. T. *Chem. Rev.* **2009**, *109*, 190–212. (f) Kobayashi, H.; Ogawa, M.; Alford, R.; Choyke, P. L.; Urano, Y. *Chem. Rev.* **2010**, *110*, 2620–2640.

(2) Loudet, A.; Burgess, K. *Chem. Rev.* **2007**, *107* (11), 4891–4932.

(3) (a) Kim, E.; Koh, M.; Ryu, J.; Park, S. B. *J. Am. Chem. Soc.* **2008**, *130*, 12206–12207. (b) Abet, V.; Nuñez, A.; Mendicuti, F.; Burgos, C.; Alvarez-Builla, J. *J. Org. Chem.* **2008**, *73*, 8800–8807. (c) Ozhalici-Unal, H.; Pow, C. L.; Marks, S. A.; Jesper, L. D.; Silva, G. L.; Shank, N. I.; Jones, E. W.; Burnette, J. M.; Berget, P. B.; Armitage, B. A. *J. Am. Chem. Soc.* **2008**, *130* (38), 12620–12621.

(4) Alexander, M. D.; et al. *ChemBioChem* **2006**, *7*, 409–416.

(5) (a) Ramesh, C.; Bryant, B.; Nayak, T.; Revankar, C. M.; Anderson, T.; Carlson, K. E.; Katzenellenbogen, J. A.; Sklar, L. A.; Norenberg, J. P.; Prossnitz, E. R.; Arterburn, J. B. *J. Am. Chem. Soc.* **2006**, *128*, 14476–14477. (b) Nayak, T. K.; Hathaway, H. J.; Ramesh, C.; Arterburn, J. B.; Dai, D.; Sklar, L. A.; Norenberg, J. P.; Prossnitz, E. R. *J. Nucl. Med.* **2008**, *49* (6), 978–986.

(6) (a) Dubs, P.; Bourel-Bonnet, L.; Subra, G.; Blanpain, A.; Melnyk, O.; Pinel, A. M.; Gras-Masse, H.; Martinez, J. *J. Comb. Chem.* **2007**, *9*, 973–981. (b) Kurpiers, T.; Mootz, H. D. *Angew. Chem., Int. Ed.* **2009**, *48*, 1729–1731. (c) Dilek, O.; Bane, S. L. *Tetrahedron Lett.* **2008**, *49*, 1413–1416. (d) Tang, W.; Xiang, Y.; Tong, A. *J. Org. Chem.* **2009**, *74*, 2163–2166. (e) Dirksen, A.; Yegneswaran, S.; Dawson, P. E. *Angew. Chem., Int. Ed.* **2010**, *49*, 2023–2027.

(7) SoluLink: http://www.solulink.com/productindex.php.

(8) (a) Umezawa, K.; Nakamura, Y.; Makino, H.; Citterio, D.; Suzuki, K. *J. Am. Chem. Soc.* **2008**, *130*, 1550–1551. (b) Zhang, G.; Chen, J.; Payne, S.; Kooi, S. E.; Demas, J. N.; Fraser, C. L. *J. Am. Chem. Soc.* **2007**, *129*, 8942–8943. (c) Gorman, A.; Killoran, J.; O'Shea, C.; Kenna, T.; Gallagher, W. M.; O'Shea, D. F. *J. Am. Chem. Soc.* **2004**, *126*, 10619–10631. (d) Zhou, Y.; Xiao, Y.; Chi, S.; Qian, X. *Org. Lett.* **2008**, *10*, 633–636. (e) Han, J.; Loudet, A.; Barhoumi, R.; Burghardt, R. C.; Burgess, K. *J. Am. Chem. Soc.* **2009**, *131*, 1642–1643. (f) Tasior, M.; O'Shea, D. F. *Bioconjugate Chem.* **2010**, *21*, 1130–1133.

(9) (a) Chang, P. V.; Prescher, J. A.; Hangauer, M. J.; Bertozzi, C. R. *J. Am. Chem. Soc.* **2007**, *129*, 8400–8401. (b) Shao, F.; Weissleder, R.; Hilderbrand, S. A. *Bioconjugate Chem.* **2008**, *19*, 2487–2491. (c) Tsou, L. K.; Zhang, M. M.; Hang, H. C. *Org. Biomol. Chem.* **2009**, *7*, 5055–5058. (d) Jewett, J. C.; Sletten, E. M.; Bertozzi, C. R. *J. Am. Chem. Soc.* **2010**, *132*, 3688–3690.

(10) Tahtaoui, C.; Thomas, C.; Rohmer, F.; Klotz, P.; Duportail, G.; Mély, Y.; Bonnet, D.; Hibert, M. *J. Org. Chem.* **2007**, *72*, 269–272.

(11) (a) Debonis, S.; Skoufias, D. A.; Lebeau, L.; Lopez, R.; Robin, G.; Margolis, R. L.; Wade, R. H.; Kozielski, F. *Mol. Cancer Ther.* **2004**, *3*, 1079–1090. (b) Debonis, S.; Skoufias, D. A.; Indorato, R. L.; Liger, F.; Marquet, B.; Laggner, C.; Joesph, B.; Kozielski, F. *J. Med. Chem.* **2008**, *51*, 1115–1125. (c) Ogo, N.; Oishi, S.; Matsuno, K.; Sawada, J.; Fujii, N.; Asai, A. *Bioorg. Med. Chem. Lett.* **2007**, *17*, 3921–3924.

(12) (a) Brier, S.; Lemaire, D.; DeBonis, S.; Forest, E.; Kozielski, F. *Biochemistry* **2004**, *43*, 13072–13082. (b) Skoufias, D. A.; Debonis, S.; Saoudi, Y.; Lebeau, L; Crevel, I.; Cross, R.; Wade, R. H; Hackney, D.; Kozielski, F. *J. Biol. Chem.* **2006**, *281*, 17559–17569.

(13) Peterson, J. R.; Mitchison, T. J. *Chem. Biol.* **2002**, *9*, 1275–1295.

(14) Verbrugge, S.; Lechner, B.; Woehlke, G.; Peterman, E. J. G. *Biophys. J.* **2009**, *97*, 173–182.
(15) Johnson, I. *Histochem. J.* **1998**, *30*, 123–140.
(16) Puckett, C. A.; Barton, J. K. *J. Am. Chem. Soc.* **2009**, *131*, 8738–8739.
(17) Lemcke, S.; Hönnscheidt, C.; Waschatko, G.; Bopp, A.; Lütjohann, D.; Bertram, N.; Gehrig-Burger, K. *Mol. Cell. Endocrinol.* **2010**, *314*, 31–40.
(18) Rickert, E. L.; Oriana, S.; Hartman-Frey, C.; Long, X.; Webb, T. T.; Nephew, K. P.; Weatherman, R. V. *Bioconjugate Chem.* **2010**, *21*, 903–910.